

Molecular beam epitaxy growth of iodide thin films

Xinqiang Cai(蔡新强), Zhilin Xu(徐智临), Shuai-Hua Ji(季帅华), Na Li(李娜), and Xi Chen(陈曦)

Citation: Chin. Phys. B, 2021, 30 (**2**): 028102. DOI: 10.1088/1674-1056/abcf93
Journal homepage: http://cpb.iphy.ac.cn; http://iopscience.iop.org/cpb

What follows is a list of articles you may be interested in

Epitaxial growth and air-stability of monolayer Cu_2Te

K Qian(钱凯), L Gao(高蕾), H Li(李航), S Zhang(张帅), J H Yan(严佳浩), C Liu(刘晨), J O Wang(王嘉鸥), T Qian(钱天), H Ding(丁洪), Y Y Zhang(张余洋), X Lin(林晓), S X Du(杜世萱), H-J Gao(高鸿钧)
Chin. Phys. B, 2020, 29 (**1**): 018104. DOI: 10.1088/1674-1056/ab5781

Effect of growth temperature of $GaAs_xSb_{1-x}$ metamorphic buffer layer on electron mobility of InAs/AlSb heterostructures grown on Si substrate

Jing Zhang(张静), Hong-Liang Lv(吕红亮), Hai-Qiao Ni(倪海桥), Shi-Zheng Yang(杨施政), Xiao-Ran Cui(崔晓然), Zhi-Chuan Niu(牛智川), Yi-Men Zhang(张义门), Yu-Ming Zhang(张玉明)
Chin. Phys. B, 2019, 28 (**11**): 118102. DOI: 10.1088/1674-1056/ab4d49

Molecular beam epitaxial growth of high quality InAs/GaAs quantum dots for 1.3-μ quantum dot lasers

Hui-Ming Hao(郝慧明), Xiang-Bin Su(苏向斌), Jing Zhang(张静), Hai-Qiao Ni(倪海桥), Zhi-Chuan Niu(牛智川)
Chin. Phys. B, 2019, 28 (**7**): 078104. DOI: 10.1088/1674-1056/28/7/078104

Effects of growth temperature and metamorphic buffer on electron mobility of InAs film grown on Si substrate by molecular beam epitaxy

Jing Zhang(张静), Hongliang Lv(吕红亮), Haiqiao Ni(倪海桥), Shizheng Yang(杨施政), Xiaoran Cui(崔晓然), Zhichuan Niu(牛智川), Yimen Zhang(张义门), Yuming Zhang(张玉明)
Chin. Phys. B, 2019, 28 (**2**): 028101. DOI: 10.1088/1674-1056/28/2/028101

A review on MBE-grown HgCdSe infrared materials on GaSb (211)B substrates

Z K Zhang, W W Pan, J L Liu, W Lei
Chin. Phys. B, 2019, 28 (**1**): 018103. DOI: 10.1088/1674-1056/28/1/018103

RAPID COMMUNICATION

Molecular beam epitaxy growth of iodide thin films*

Xinqiang Cai(蔡新强)[1], Zhilin Xu(徐智临)[1], Shuai-Hua Ji(季帅华)[1], Na Li(李娜)[2,†], and Xi Chen(陈曦)[1]

[1] State Key Laboratory of Low Dimensional Quantum Physics, Department of Physics, Tsinghua University, Beijing 100084, China
[2] Key Laboratory for the Physics and Chemistry of Nanodevices, Department of Electronics, Peking University, Beijing 100871, China

(Received 14 November 2020; revised manuscript received 27 November 2020; accepted manuscript online 2 December 2020)

Study of two-dimensional (2D) magnetic materials is important for both fundamental research and application. Here we report molecular beam epitaxy growth of iodides, candidates for exhibiting 2D magnetism. Decomposition of CrI_3 is utilized to produce stable gaseous I_2 flux. Growth of MnI_2, GdI_3, and CrI_2 down to monolayer is successful achieved by co-depositing I_2 and corresponding metal atoms. The thin films of the three materials are characterized by scanning tunneling microscope and found to be insulators with bandgaps of 4.4 eV, 0.6 eV, and 3.0 eV, respectively. The film growth paves the way for further study of magnetic properties at the 2D limit.

Keywords: two-dimensional magnetism, iodide thin films, molecular beam epitaxy, scanning tunneling microscope

PACS: 81.15.Hi, 75.50.Pp, 07.79.Cz, 73.22.–f **DOI:** 10.1088/1674-1056/abcf93

Since the discovery of graphene in 2004, two-dimensional (2D) materials have been extensively studied because of their fascinating properties and potential applications in fabricating functional nanomaterials and nanodevices.[1,2] Among the various properties, 2D magnetism has drawn great attention recently. The investigation on the long-range magnetic order and other spin-related phenomena at the 2D limits may promote the development of spintronics at the nano-scale.

The 2D magnetism was first clearly confirmed in atomically thin CrI_3[3] and $Cr_2Ge_2Te_6$[4] layers, respectively. The high-quality 2D magnetic crystals are mechanically exfoliated from the layered compounds. However, the size and yield of the flakes from exfoliation potentially limit further applications. Chemical vapor deposition (CVD) is another approach to synthesize the 2D magnetic materials. In addition, it is difficult to avoid the contamination introduced in the process of exfoliation or deposition. Here we consider the molecular beam epitaxy (MBE) growth of iodides with promising long-range magnetic order in 2D limit. MBE growth in ultrahigh vacuum (UHV) can achieve much higher purity under well-controlled conditions.

In the MBE synthesis of iodides, one needs metal and iodine sources with high purity. However, the vapor pressure of elemental iodine I_2 at room temperature is as high as 0.2 torr, which is not compatible with UHV. A leak valve can be employed to dose such substance with high vapor pressure.[5] Herein we introduce a more convenient and reliable procedure to generate I_2 molecular beam, in which I_2 is thermally decomposed from pure iodides, similar to previous attempt to use FeS as sulfur source.[6] By heating selected iodides in Knudsen cell, it is possible to obtain sufficient flux of I_2. Compared with the gaseous source, the I_2 vapor from decomposition can be fine-controlled. Such procedure is universally applicable in MBE growth of iodides and can well protect the vacuum system. To demonstrate the advantage of the compound iodine source, we prepare MnI_2, GdI_3, and CrI_2 thin films down to monolayer. Further studies are needed to reveal the magnetic properties of these iodides.

The experiments were conducted on a Unisoku low-temperature scanning tunneling microscope (STM) equipped with an MBE chamber. After thin film preparation, the samples were directly transferred to STM at 78 K for characterization. The STM topographic imaging at the atomic scale was utilized to identify the crystal structures. The local density of states was measured by the scanning tunneling spectroscopy (STS) to unveil the electronic structure of the samples. Before STM measurement, the Pr–Ir alloy tips were checked and modified on the surface of Ag(111) islands grown on Si(111). The samples can also be transferred to x-ray photoelectron spectroscopy (XPS) to analyze the chemical compositions.

A good candidate for the compound iodine source needs to be stable in air and its decomposition products except I_2 should have exceedingly low vapor pressure. Furthermore, the decomposition temperature for stably producing adequate amount of I_2 vapor has to be high enough (usually above 200 °C) in order for the Knudsen cell to work in the temperature range with precise control. Among various iodides, VI_3 and CrI_3[7–10] are found to meet the requirements. After heating, they are decomposed into I_2 vapor together with solid VI_2 or CrI_2[9,10] following the formula $2MI_3(s) \leftrightharpoons 2MI_2(s) + I_2(g)$, where M represents V or Cr. We choose CrI_3 powder (Six Carbon Technology) as the I_2 source in the MBE growth. The

*Project supported by the Science Challenge Project (Grant No. TZ2016004).
†Corresponding author. E-mail: na-li07@pku.edu.cn
© 2021 Chinese Physical Society and IOP Publishing Ltd

Knudsen cell uses Al_2O_3 crucible. According to previous report,[9] the equilibrium pressure of I_2 vapor in the reaction $2CrI_3 \rightleftharpoons 2CrI_2 + I_2$ satisfies $\log[P(\text{torr})] = -8936/T + 11.832$, when the heating temperature T is between 580 K and 650 K. Extrapolation to the temperature slightly below 580 K sets the upper limit of I_2 vapor pressure as 10^{-6} torr at 230 °C and 10^{-5} torr at 260 °C. The working temperature of the Knudsen cell in our MBE growth is around this range, where the sensitivity of the vapor pressure to temperature is low enough to ensure a stable I_2 flux.

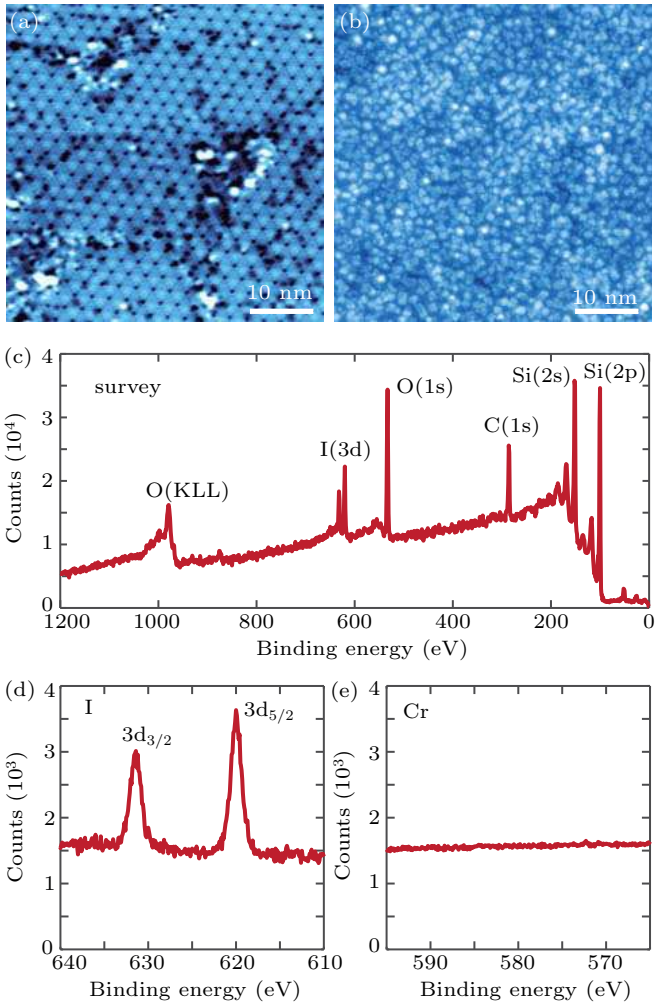


Fig. 1. STM topography (50 nm×50 nm, bias: 1.5 V, current: 20 pA) of (a) Si(111) surface with 7×7 reconstruction before deposition. (b) I_2 on Si(111) surface after deposition. (c) XPS survey of adsorbates on Si(111) surface. (d) XPS signal of iodine 3d electrons. (e) Absence of XPS signal of chromium 2p electrons.

The I_2 source was checked by deposition onto clean Si(111) surface with 7×7 reconstruction structure obtained by flashing to 1180 °C for several times. The temperature of the Knudsen cell was kept at 220 °C and the pressure was below 3×10^{-9} torr during the growth. Figures 1(a) and 1(b) show the STM topographic images of Si(111) before and after deposition, respectively. The adsorbates are clearly revealed. Besides iodine, the adsorbates could be the unwanted Cr, CrI_2, or CrI_4 (similar to VI_3, decomposition accompanied by gaseous VI_4[9]). The composition of the adsorbates was analyzed by XPS. Figure 1(c) exhibits the XPS spectrum, where peaks corresponding to I, Si, C, and O are clearly identified. The carbon and oxygen come from the air contamination because of the *ex-situ* XPS measurement. The two peaks in Fig. 1(d) at energies of 631.4 eV and 620.0 eV well match the characteristic photoemission spectra of $3d_{3/2}$ and $3d_{5/2}$ states for I_2.[11] No Cr(2p) characteristic peaks[12] have been detected (Fig. 1(e)). Generally, CrI_3 is an eligible source of iodine in MBE thin film growth.

Three typical iodides MnI_2, GdI_3, and CrI_2 with layered Van der Waals structure have been prepared by using the CrI_3 source. The three compounds are chosen according to their magnetic properties in their bulk form, which are antiferromagnetic below 3.95 K for MnI_2,[13,14] possibly antiferromagnetic below 1.5 K for GdI_3,[15] and unexplored for CrI_2. We mainly like to focus on the antiferromagnetic materials due to recent advent of antiferromagnetic spintronics.[16–18] Devices made of antiferromagnetic materials are stable against external magnetic field and have little influence on the devices nearby. For the purpose of device applications, it is indispensable to prepare antiferromagnetic thin films with high quality.

In the experiments, the Mn, Gd, or Cr metals (Alfa Aesar, purity over 99.9%) were evaporated from Knudsen cells. The co-deposited metal atoms and I_2 molecules react to form thin films on graphitized 6H-SiC(0001) (n-doped, resistivity $\sim 0.1\ \Omega\cdot$cm) substrate kept at elevated temperature. The substrate is terminated with monolayer or bilayer graphene by heating to 1400 °C in advance. During growth, the pressure was below 3×10^{-9} torr. The nominal flux of iodine is much higher than that of the metal atoms (the ratio is over 10 : 1) to ensure sufficient reaction on the substrate surface.

Figure 2 shows the growth and characterization of MnI_2 films down to monolayer. Bulk MnI_2 is antiferromagnetic and ferroelectric at low temperature, with a polarization direction tunable by magnetic field.[19] Figure 2(a) exhibits the crystal structure of MnI_2, which is isostructural to CdI_2. The lattice constants are $a = b = 4.146$ Å, and $c = 6.829$ Å.[13] The MBE growth of MnI_2 film helps to study the magnetic order and multiferroicity at 2D limit. To achieve high quality MnI_2 films, the temperatures of Mn and CrI_3 sources were set at 680 °C and 236 °C, respectively, while the substrate at 210 °C. Figure 2(b) shows the STM topography of a sample after 60 min of deposition. Edge of the monolayer films is highlighted by yellow lines. The triangular lattice is observed in the atomic resolution STM image (Fig. 2(c)). The in-plane lattice constants are measured to be $a = b = 4.14$ Å. The apparent height of the MnI_2 monolayer above graphene is 6.8 Å (inset of Fig. 2(b)). The measured lattice parameters well match those of the bulk material. Further STS measurement (Fig. 2(d)) demonstrates that monolayer MnI_2 is an insulator with a bandgap of about 4.4 eV.

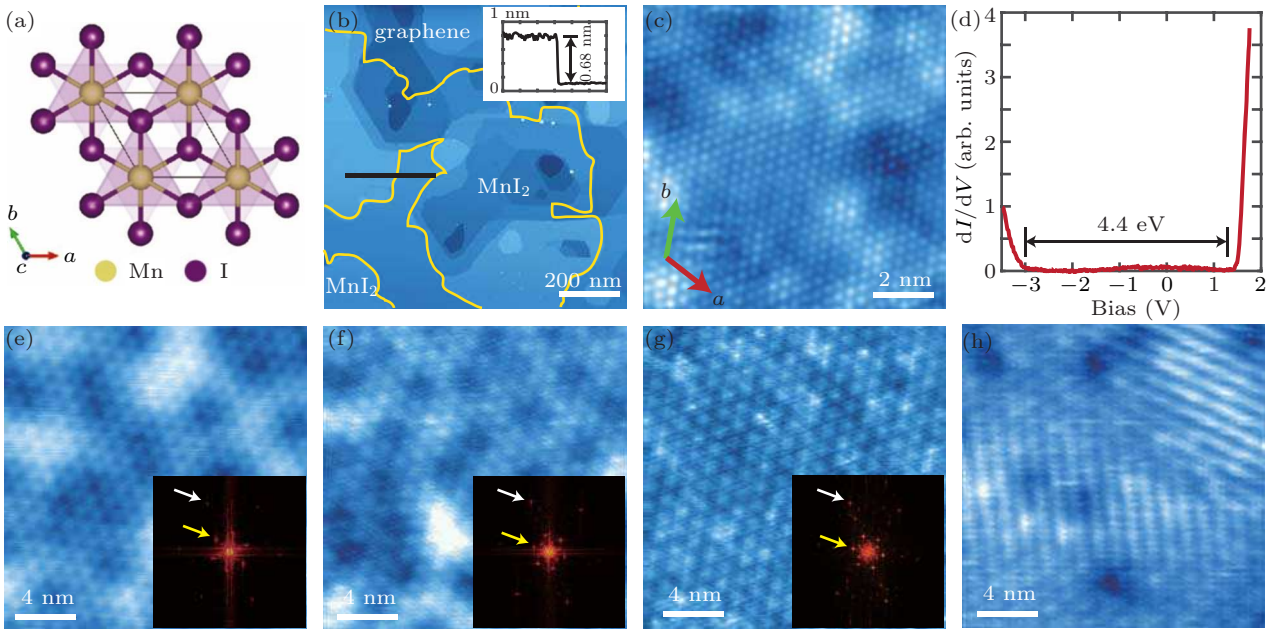


Fig. 2. (a) Top view of single layer MnI_2. I atoms above and below Mn atomic plane form two triangular lattices. (b) STM topography of MnI_2 films (1000 nm×1000 nm; bias: 3 V; current: 20 pA). Edge of MnI_2 film is highlighted by yellow line. Inset shows the height profile along the black line. (c) STM atomic resolution of MnI_2 (10 nm×10 nm; bias: 1 V; current: 100 pA). (d) STS of monolayer MnI_2 (bias: 1.7 V; current: 100 pA). (e)–(g) STM images (20 nm×20 nm; bias: 1.9 V (e), 1.8 V (f), −0.5 V (g); current: 100 pA) of Moiré patterns on monolayer MnI_2 with FFT inset. The periods are 1.19 nm, 1.28 nm, and 1.32 nm, respectively. (h) STM image of stripe pattern on monolayer MnI_2 (bias: 1.5 V; current: 100 pA).

Monolayer MnI_2 on bilayer graphene exhibits various Moiré patterns depending on the twisted angles between MnI_2 and graphene. Three types of Moiré patterns are clearly resolved in the STM images (Figs. 2(e)–2(g)). In the corresponding fast Fourier transform (FFT, see the insets), the peaks arising from the triangular lattice and the Moiré patterns are indicated by white and yellow arrows. The periods and the twisted angles relative to graphene of the three Moiré patterns are 1.19 nm, 1.28 nm, 1.32 nm and 5.0°, 2.5°, 1.0°, respectively. Occasionally, a twisted angle as large as 30° is also observed (not shown). Apart from the Moiré patterns, monolayer MnI_2 sometime shows a stripe structure (Fig. 2(h)) with period between 1.12 nm and 1.20 nm. The orientation of the stripes has no obvious relation with the lattice and the edge of the film. The origin of the stripe structure is not understood yet.

Figure 3 shows the growth and characterization of GdI_3 films down to monolayer. Bulk GdI_3 is isostructural to BiI_3. A unit cell contains three single-layers of GdI_3. A single layer of GdI_3 has one layer of Gd sandwiched between two layers of I atoms as shown in Fig. 3(a). The lattice parameters are $a = b = 7.539$ Å and $c = 20.83$ Å.[20] The GdI_3 film in Fig. 3(b) took 30 min to prepare under the condition of Gd source at 1080 °C, CrI_3 at 225 °C, and the substrate at 500 °C. The growth window of the substrate temperature is rather large and can be as low as 300 °C. As shown in the atomic resolution STM image in Fig. 3(c), the Gd atoms form a honeycomb lattice. The in-plane lattice constant is measured to be 7.54 Å and is consistent with that of bulk GdI_3. The apparent height of GdI_3 monolayer above graphene is 6.5 Å (inset of Fig. 3(b)), which is close to $c/3 = 6.94$ Å. The monolayer is found to be an insulator by the STS measurement (Fig. 3(d)) with a bandgap of about 0.6 eV. The spin structure needs further investigation.

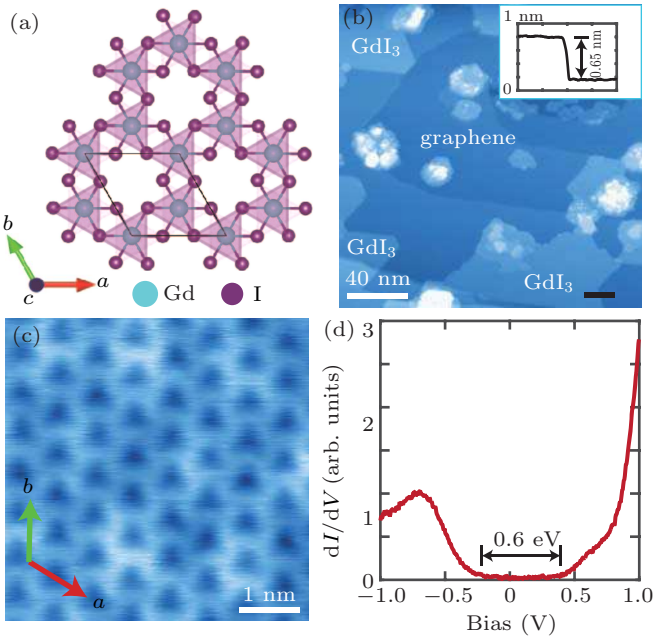


Fig. 3. (a) Top view of GdI_3 lattice. (b) STM topography (200 nm×200 nm; bias: 3 V; current: 20 pA) of GdI_3 films. Inset shows the height profile along the black line when the sample bias is 2.0 V. (c) STM atomic resolution (10 nm×10 nm; bias: 1 V; current: 100 pA) of GdI_3. Inset shows the honeycomb lattice of monolayer GdI_3. (d) STS of monolayer GdI_3 (bias: 1.0 V; current: 100 pA).

Finally, we try the growth of CrI_2 thin film. A single layer of CrI_2 consists of one layer of Cr sandwiched between two layers of I atoms. The bulk crystal has two configu-

rations. One is similar to that of the 1T-transition metal dichalcogenides but elongated along the b axis (Fig. 4(a)). It belongs to the monoclinic crystal structure with the lattice constants of $a = 7.545$ Å, $b = 3.929$ Å, $c = 7.505$ Å, $\alpha = \gamma = 90°$, $\beta = 115.52°$.[21] The inversion symmetry is preserved within single layer CrI_2. Another one (Fig. 4(b)) is orthorhombic with the lattice constants of $a = 7.560$ Å, $b = 3.915$ Å, $c = 13.553$ Å, $\alpha = \beta = \gamma = 90°$, which breaks the inversion symmetry within single layer CrI_2.[22] In both structures, a Cr atom is surrounded by six nearest-neighboring iodine atoms. In the thin film growth, Cr (at 1000 °C) and I_2 released from CrI_3 (at 208 °C) were co-deposited on graphitized SiC (300 °C) for 40 min. Figure 4(c) shows the STM topography of the monolayer film (surrounded by the yellow line). The coverage of the film is lower than one. The apparent height of the film is 7.0 Å (see inset of Fig. 4(c)) when the sample bias is set at 2.0 V. The atomic resolution image (Fig. 4(d)) reveals the single I atoms on the topmost layer. The lattice constants are $a = 7.46$ Å, $b = 3.91$ Å, slightly different from the bulk ones due to unidentified origin . The two different crystal configurations cannot be distinguished by the STM image because of their small difference in the lattice constants. The STS (Fig. 4(e)) shows that CrI_2 monolayer is an insulator with bandgap of about 3.0 eV.

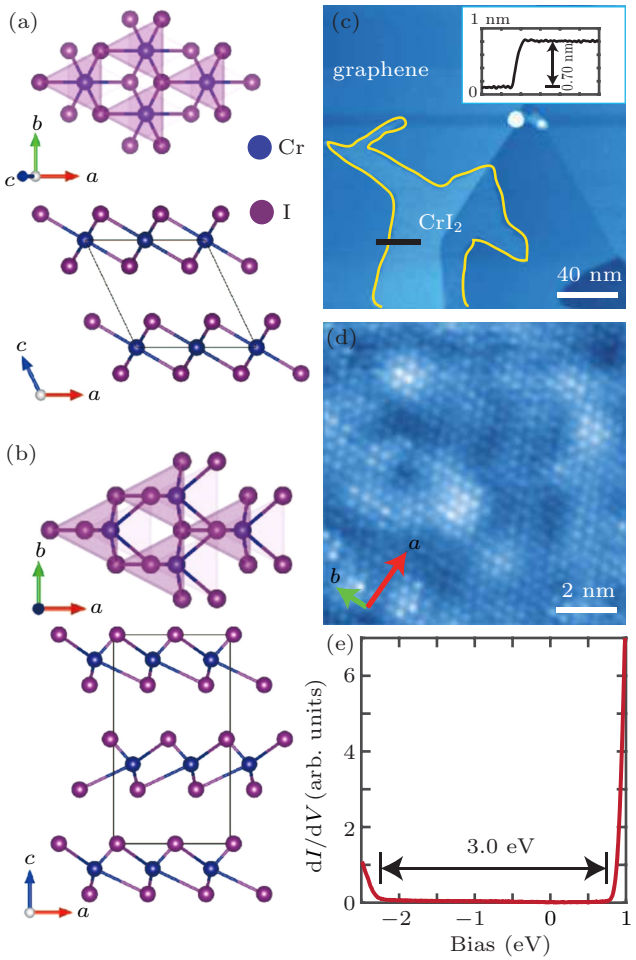


Fig. 4. (a) Top and side views of CrI_2 crystal.[21] (b) Top and side views of CrI_2 from Ref. [22]. (c) STM topography (200 nm×200 nm; bias: 4 V; current: 20 pA) of CrI_2 films. Edge of CrI_2 film is highlighted by yellow line. Inset shows height profile along the black line when sample bias is 2.0 V. (d) STM atomic resolution (10 nm×10 nm; bias: 0.4 V; current: 100 pA) of CrI_2. (e) STS of monolayer CrI_2 (bias: 1 V; current: 100 pA).

In conclusion, we demonstrate a reliable growth method of iodides by MBE. The thermally decomposed CrI_3 releases very pure I_2 vapor, whose flux can be well controlled by the heating temperature. The effectiveness of the iodine source is demonstrated by the growth of MnI_2, GdI_3, and CrI_2 thin films. It is expected to promote the study on magnetism at the 2D limit.

References

[1] Novoselov K S, Geim A K, Morozov S V, Jiang D, Katsnelson M I, Grigorieva I V, Dubonos S V and Firsov A A 2005 *Nature* **438** 197

[2] Zhang Y B, Tan Y W, Stormer H L and Kim P 2005 *Nature* **438** 201

[3] Huang B, Clark G, Navarro-Moratalla E, Klein D R, Cheng R, Seyler, K L, Zhong D, Schmidgall E, McGuire M A, Cobden D H, Yao W, Xiao D, Jarillo-Herrero P and Xu X D. 2017 *Nature* **546** 270

[4] Gong C, Li L, Li Z L, Ji H W, Stern A, Xia Y, Cao T, Bao W, Wang C Z, Wang Y, Qiu Z Q, Cava R J, Louie S G, Xia J and Zhang X 2017 *Nature* **546** 265

[5] Peng L, Zhao J Z, Cai M, Hua G Y, Liu Z Y, Xia H N, Yuan Y, Zhang W H, Xu G, Zhao L X, Zhu Z W, Xiang T and Fu Y S 2020 *Phys. Rev. Research* **2** 023264

[6] Lin H C, Huang W T, Zhao K, Qiao S, Liu Z, Wu J, Chen X and Ji S H 2018 *Nano. Research* **11** 4722

[7] Cai X Q, Xu Z L, Zhou H, Ren J, Li N, Meng S, Ji S H and Chen X 2020 *Phys. Rev. Materials* **4** 064003

[8] Li P G, Wang C, Zhang J H, Chen S W, Guo D H, Ji W and Zhong D Y 2020 *Sci. Bull.* **65** 1064

[9] Berry K O, Smardzewski R R and McCarley R E 1969 *Inorg. Chem.* **8** 1994

[10] Handy L L and Gregory N W 1950 *J. Am. Chem. Soc.* **72** 5049

[11] Sherwood and Peter M A 1976 *J. Chem. Soc. Faraday Trans. II* **72** 1805

[12] Salvi A M, Castle J E, Watts J F and Desimoni E 1995 *Appl. Surf. Sci.* **90** 333

[13] Cable J W, Wilkinson M K, Wollan E O and Koehler W C 1962 *Phys. Rev.* **125** 1860

[14] Sato T, Kadowaki H and Iio K 1995 *Physica B: Condensed Matter* **213–214** 224

[15] Hovi V, Vuola R and Salmenperä L J 1970 *J. Low. Temp. Phys.* **2** 383

[16] Jungwirth T, Marti X, Wadley P and Wunderlich J 2016 *Nat. Nanotechnol.* **11** 231

[17] Baltz V, Manchon A, Tsoi M, Moriyama T, Ono T and Tserkovnyak T 2018 *Rev. Mod. Phys.* **90** 015005

[18] Jungwirth T, Sinova J, Manchon A, Marti X, Wunderlich J and Felser C 2018 *Nat. Phys.* **14** 200

[19] Kurumaji T, Seki S, Ishiwata S, Murakawa H, Tokunaga Y, Kaneko Y and Tokura Y 2011 *Phys. Rev. Lett.* **106** 167206

[20] Asprey L B, Keenan T K and Kruse F H 1964 *Inorg. Chem.* **3** 1137

[21] Tracy J W, Gregory N W, Stewart J M and Lingafelter E C 1962 *Acta Cryst.* **15** 460

[22] Besrest F and Jaulmes S 1973 *Acta Cryst. B* **29** 1560